
Deep Conditional Gaussian Mixture Model for Constrained Clustering

Laura Manduchi

Department of Computer Science
ETH Zürich
laura.manduchi@inf.ethz.ch

Kieran Chin-Cheong

Department of Computer Science
ETH Zürich
kieran.chincheong@inf.ethz.ch

Holger Michel

Department of Neonatology
University Children's Hospital Regensburg (KUNO)
University of Regensburg, Germany
holger.michel@barmherzige-regensburg.de

Sven Wellmann

Department of Neonatology
University Children's Hospital Regensburg (KUNO)
University of Regensburg, Germany
sven.wellmann@klinik.uni-regensburg.de

Julia E. Vogt

Department of Computer Science
ETH Zürich
julia.vogt@inf.ethz.ch

Abstract

Constrained clustering has gained significant attention in the field of machine learning as it can leverage prior information on a growing amount of only partially labeled data. Following recent advances in deep generative models, we propose a novel framework for constrained clustering that is intuitive, interpretable, and can be trained efficiently in the framework of stochastic gradient variational inference. By explicitly integrating domain knowledge in the form of probabilistic relations, our proposed model (DC-GMM) uncovers the underlying distribution of data conditioned on prior clustering preferences, expressed as *pairwise constraints*. These constraints guide the clustering process towards a desirable partition of the data by indicating which samples should or should not belong to the same cluster. We provide extensive experiments to demonstrate that DC-GMM shows superior clustering performances and robustness compared to state-of-the-art deep constrained clustering methods on a wide range of data sets. We further demonstrate the usefulness of our approach on two challenging real-world applications.

1 Introduction

The ever-growing amount of data and the time cost associated with its labeling has made clustering a relevant task in the field of machine learning. Yet, in many cases, a fully unsupervised clustering algorithm might naturally find a solution that is not consistent with the domain knowledge (Basu et al., 2008). In medicine, for example, clustering could be driven by unwanted bias, such as the type of machine used to record the data, rather than more informative features. Moreover, practitioners often have access to prior information about the types of clusters that are sought, and a principled method to guide the algorithm towards a desirable configuration is then needed. Therefore, *constrained clustering* has a long history in machine learning as it enforces desirable clustering properties by

incorporating domain knowledge, in the form of *instance-level* constraints (Wagstaff & Cardie, 2000), into the clustering objective.

A variety of methods have been proposed to extend deterministic deep clustering algorithms, such as DEC (Xie et al., 2016), to force the clustering process to be consistent with given constraints (Ren et al., 2019; Zhang et al., 2019). This results in a wide range of empirically motivated loss functions that are rather obscure in their underlying assumptions. Further, they are unable to uncover the distribution of the data, preventing them from being extended to other tasks beyond clustering, such as Bayesian model validation, outlier detection, and data generation (Min et al., 2018). Thus, we restrict our search for a constrained clustering approach to the class of deep generative models. Although these models have been successfully used in the unsupervised setting (Jiang et al., 2017; Dilokthanakul et al., 2016), their application to constrained clustering has been under-explored.

In this work we propose a novel probabilistic approach to constrained clustering, the Deep Conditional Gaussian Mixture Model (DC-GMM), that employs a deep generative model to uncover the underlying data distribution conditioned on domain knowledge, expressed in the form of pairwise constraints. Our model assumes a Conditional Mixture-of-Gaussians prior on the latent representation of the data. That is, a Gaussian Mixture Model conditioned on the user’s clustering preferences, based e.g. on domain knowledge. These preferences are expressed as Bayesian prior probabilities with varying degrees of uncertainty. By integrating prior information in the generative process of the data, our model can guide the clustering process towards the configuration sought by the practitioners. Following recent advances in variational inference (Kingma & Welling, 2014; Rezende et al., 2014), we derive a scalable and efficient training scheme using amortized inference.

Our main contributions are as follows: (i) We propose a new paradigm for constrained clustering (DC-GMM) to incorporate instance-level clustering preferences, with varying degrees of certainty, within the Variational Auto-Encoder (VAE) framework. (ii) We provide a thorough empirical assessment of our model. In particular, we show that (a) a small fraction of prior information remarkably increases the performance of DC-GMM compared to unsupervised variational clustering methods, (b) our model shows superior clustering performance compared to state-of-the-art deep constrained clustering models on a wide range of data sets and, (c) our model proves to be robust against noise as it can easily incorporate the uncertainty of the given constraints. (iii) Additionally, we demonstrate on two challenging real-world applications that our model can drive the clustering performance towards different desirable configurations, depending on the constraints used.

2 Deep Conditional Gaussian Mixture Model

In the following section, we propose a probabilistic approach to constrained clustering (DC-GMM) that incorporates clustering preferences, with varying degrees of certainty, in a VAE-based setting. In particular, we first describe the generative assumptions of the data conditioned on the domain knowledge, for which VaDE (Jiang et al., 2017) and GMM-VAE (Dilokthanakul et al., 2016) are special cases. We then define a concrete prior formulation to incorporate pairwise constraints and we derive a new objective, the Conditional ELBO, to train the model in the framework of stochastic gradient variational Bayes. Finally, we discuss the optimization procedure and the computational complexity of the proposed algorithm.

2.1 The Generative Assumptions

Let us consider a data set $\mathbf{X} = \{\mathbf{x}_i\}_{i=1}^N$ consisting of N samples with $\mathbf{x}_i \in \mathbb{R}^M$ that we wish to cluster into K groups according to instance-level prior information encoded as $\mathbf{W} \in \mathbb{R}^{N \times N}$. For example, we may know *a priori* that certain samples should (or should not) be clustered together. However, the prior information often comes from different sources with different noise levels. As an example, the instance-level annotations could be obtained from both very experienced domain experts and less experienced users. Hence, \mathbf{W} should

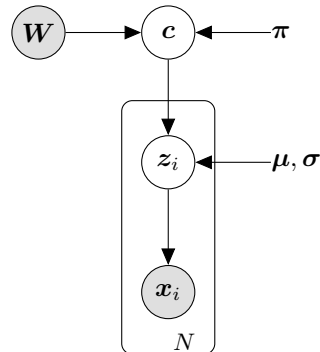


Figure 1: The proposed graphical model.

encode both our prior knowledge of the data set, expressed in the form of constraints, and its degree of confidence.

We assume the data is generated from a random process consisting of three steps, as depicted in Fig. 1. First, the cluster assignments $\mathbf{c} = \{c_i\}_{i=1}^N$, with $c_i \in \{1, \dots, K\}$, are sampled from a distribution conditioned on the prior information:

$$\mathbf{c} \sim p(\mathbf{c}|\mathbf{W}; \boldsymbol{\pi}) \quad (1)$$

The prior distribution of the cluster assignments without domain knowledge \mathbf{W} , i.e. $p(\mathbf{c})$, follows a categorical distribution with mixing parameters $\boldsymbol{\pi}$. Second, for each cluster assignment c_i , a continuous latent embedding, $\mathbf{z}_i \in \mathbb{R}^D$, is sampled from a Gaussian distribution, whose mean and variance depend on the selected cluster c_i . Finally, the sample \mathbf{x}_i is generated from a distribution conditioned on \mathbf{z}_i . Given c_i , the generative process can be summarized as:

$$\mathbf{z}_i \sim p(\mathbf{z}_i|c_i) = \mathcal{N}(\mathbf{z}_i|\boldsymbol{\mu}_{c_i}, \boldsymbol{\sigma}_{c_i}^2 \mathbb{I}) \quad (2)$$

$$\mathbf{x}_i \sim p_\theta(\mathbf{x}_i|\mathbf{z}_i) = \begin{cases} \mathcal{N}(\mathbf{x}_i|\boldsymbol{\mu}_{x_i}, \boldsymbol{\sigma}_{x_i}^2 \mathbb{I}) & \text{if real-valued} \\ \text{Ber}(\boldsymbol{\mu}_{x_i}) & \text{if binary} \end{cases} \quad (3)$$

where $\boldsymbol{\mu}_{c_i}$ and $\boldsymbol{\sigma}_{c_i}^2$ are mean and variance of the Gaussian distribution corresponding to cluster c_i in the latent space. In the case where \mathbf{x} is real-valued then $[\boldsymbol{\mu}_{x_i}, \boldsymbol{\sigma}_{x_i}^2] = f(\mathbf{z}_i; \boldsymbol{\theta})$, if \mathbf{x} is binary then $\boldsymbol{\mu}_{x_i} = f(\mathbf{z}_i; \boldsymbol{\theta})$. The function $f(\mathbf{z}; \boldsymbol{\theta})$ denotes a neural network, called *decoder*, parametrized by $\boldsymbol{\theta}$.

It is worth noting that, given \mathbf{W} , the cluster assignments are not necessarily independent, i.e. there might be certain $i, j \in \{1, \dots, N\}$ for which $(c_i \not\perp c_j|\mathbf{W})$. This important detail prevents the use of standard optimization procedure and it will be explored in the following Sections. On the contrary, if there is no prior information, that is $p(\mathbf{c}|\mathbf{W}) = p(\mathbf{c}) = \prod_i p(c_i) = \prod_i \text{Cat}(c_i|\boldsymbol{\pi})$, the cluster assignments are independent and identical distributed. In that particular case, the generative assumptions described above are equal to those of Jiang et al. (2017); Dilokthanakul et al. (2016) and the parameters of the model can be learned using the unsupervised VaDE method. As a result, VaDE (or GMM-VAE) can be seen as a special case of our framework.

2.2 Conditional Prior Probability with Pairwise Constraints

We incorporate the clustering preference through the conditional probability $p(\mathbf{c}|\mathbf{W})$. We focus on pairwise constraints consisting of *must-links*, if two samples are believed to belong to the same cluster, and *cannot-links*, otherwise. However, different types of constraints can be included, for example, triple-constraints (see Appendix C).

Definition 1. Given a dataset $\mathbf{X} = \{\mathbf{x}_i\}_{i=1}^N$, the pairwise prior information $\mathbf{W} \in \mathbb{R}^{N \times N}$ is defined as a symmetric matrix containing the pairwise preferences and confidence. In particular

$$\mathbf{W}_{i,j} \begin{cases} > 0 & \text{if there is a must-link constraint between } \mathbf{x}_i \text{ and } \mathbf{x}_j \\ = 0 & \text{if there is no prior information on samples } \mathbf{x}_i \text{ and } \mathbf{x}_j \\ < 0 & \text{if there is a cannot-link constraint between } \mathbf{x}_i \text{ and } \mathbf{x}_j, \end{cases}$$

where the value $|\mathbf{W}_{i,j}| \in [0, \infty)$ reflects the degree of certainty in the constraint.

Definition 2. Given the pairwise prior information \mathbf{W} , the conditional prior probability $p(\mathbf{c}|\mathbf{W}; \boldsymbol{\pi})$ is defined as:

$$p(\mathbf{c}|\mathbf{W}; \boldsymbol{\pi}) := \frac{\prod_i \pi_{c_i} h_i(\mathbf{c}; \mathbf{W})}{\sum_{\mathbf{c}} \prod_j \pi_{c_j} h_j(\mathbf{c}; \mathbf{W})} = \frac{1}{\Omega(\boldsymbol{\pi})} \prod_i \pi_{c_i} h_i(\mathbf{c}; \mathbf{W}), \quad (4)$$

where $\boldsymbol{\pi} = \{\pi_k\}_{k=1}^K$ are the weights associated to each cluster, c_i is the cluster assignment of sample \mathbf{x}_i , $\Omega(\boldsymbol{\pi})$ is the normalization factor and $h_i(\mathbf{c}; \mathbf{W})$ is a weighting function of the form

$$h_i(\mathbf{c}; \mathbf{W}) = \prod_{j \neq i} \exp(\mathbf{W}_{i,j} \delta_{c_i c_j}). \quad (5)$$

It follows that $h_i(\mathbf{c}; \mathbf{W})$ assumes large values if c_i agrees with our belief with respect to \mathbf{c} and low values otherwise. If $\mathbf{W}_{i,j} \rightarrow -\infty$ then \mathbf{x}_i and \mathbf{x}_j must be assigned to different clusters otherwise

$p(\mathbf{c}|\mathbf{W}) \rightarrow 0$ (*hard* constraint). On the other hand, smaller values indicate a *soft preference* as they admit some degree of freedom in the model. An heuristic to select $|\mathbf{W}_{i,j}|$ is presented in Sec 4.

The conditional prior probability with pairwise constraints has been successfully used by traditional clustering methods in the past (Lu & Leen, 2004), but to the best of our knowledge, it has never been applied in the context of deep generative models. It can also be seen as the posterior of the superparamagnetic clustering method (Blatt et al., 1996), with loss function given by a fully connected Potts model (Wu, 1982).

2.3 Conditional Evidence Lower Bound

Given the data generative assumptions illustrated in Sec. 2.1, the objective is to infer the parameters of the model, θ , π , and $\nu = \{\mu_c, \sigma_c^2\}_{c=1}^K$, given both the observed data \mathbf{X} and the pairwise prior information on the cluster assignments \mathbf{W} . This could be achieved by maximizing the marginal log-likelihood conditioned on \mathbf{W} , that is:

$$\log p(\mathbf{X}|\mathbf{W}) = \log \int_{\mathbf{Z}} \sum_{\mathbf{c}} p(\mathbf{X}, \mathbf{Z}, \mathbf{c}|\mathbf{W}), \quad (6)$$

where $\mathbf{Z} = \{\mathbf{z}_i\}_{i=1}^N$ is the collection of the latent embeddings corresponding to the data set \mathbf{X} . The conditional joint probability is derived from Eq. 2 and Eq. 3 and can be factorized as:

$$p(\mathbf{X}, \mathbf{Z}, \mathbf{c}|\mathbf{W}) = p_{\theta}(\mathbf{X}|\mathbf{Z})p(\mathbf{Z}|\mathbf{c}; \nu)p(\mathbf{c}|\mathbf{W}; \pi) = p(\mathbf{c}|\mathbf{W}; \pi) \prod_{i=1}^N p_{\theta}(\mathbf{x}_i|\mathbf{z}_i)p(\mathbf{z}_i|\mathbf{c}_i; \nu). \quad (7)$$

Since the conditional log-likelihood is intractable, we derive an alternative tractable objective.

Definition 3. \mathcal{L}_C , the *Conditional ELBO (C-ELBO)*, is defined as

$$\mathcal{L}_C(\theta, \phi, \nu, \pi, \mathbf{X}|\mathbf{W}) := \mathbb{E}_{q_{\phi}(\mathbf{Z}|\mathbf{X})} [\log p_{\theta}(\mathbf{X}|\mathbf{Z})] - D_{KL}(q_{\phi}(\mathbf{Z}, \mathbf{c}|\mathbf{X}) \| p(\mathbf{Z}, \mathbf{c}|\mathbf{W}; \nu, \pi)), \quad (8)$$

with $q_{\phi}(\mathbf{Z}, \mathbf{c}|\mathbf{X})$ being the following amortized mean-field variational distribution:

$$q_{\phi}(\mathbf{Z}, \mathbf{c}|\mathbf{X}) = q_{\phi}(\mathbf{Z}|\mathbf{X})p(\mathbf{c}|\mathbf{Z}; \nu, \pi) = \prod_{i=1}^N q_{\phi}(\mathbf{z}_i|\mathbf{x}_i)p(\mathbf{c}_i|\mathbf{z}_i; \nu, \pi). \quad (9)$$

The first term of the Conditional ELBO is known as the *reconstruction term*, similarly to the VAE. The second term, on the other hand, is the Kullback-Leibler (KL) divergence between the variational posterior and the Conditional Gaussian Mixture prior. By maximizing the C-ELBO, the variational posterior mimics the true conditional probability of the latent embeddings and the cluster assignments. This results in enforcing the latent embeddings to follow a Gaussian mixture that agrees on the clustering preferences.

From Definition 3 and Equations 6 and 7, we can directly derive Lemma 1:

Lemma 1. *It holds that*

1. The C-ELBO \mathcal{L}_C is a lower bound of the marginal log-likelihood conditioned on \mathbf{W} , that is

$$\log p(\mathbf{X}|\mathbf{W}) \geq \mathcal{L}_C(\theta, \phi, \nu, \pi, \mathbf{X}|\mathbf{W}).$$

2. $\log p(\mathbf{X}|\mathbf{W}) = \mathcal{L}_C(\theta, \phi, \nu, \pi, \mathbf{X}|\mathbf{W})$ if and only if $q_{\phi}(\mathbf{Z}, \mathbf{c}|\mathbf{X}) = p(\mathbf{Z}, \mathbf{c}|\mathbf{X}, \mathbf{W})$.

For the proof we refer to the Appendix B. It is worth noting that in Eq. 9, the variational distribution does not depend on \mathbf{W} . This approximation is used to retain a mean-field variational distribution when the cluster assignments, conditioned on the prior information, are not independent (Sec 2.1), that is when $p(\mathbf{c}|\mathbf{W}) \neq \prod_i p(\mathbf{c}_i|\mathbf{W})$. Additionally, the probability $p(\mathbf{c}_i|\mathbf{z}_i)$ can be easily computed using the Bayes Theorem, yielding

$$p(\mathbf{c}_i|\mathbf{z}_i; \nu, \pi) = \frac{\mathcal{N}(\mathbf{z}_i|\mu_{c_i}, \sigma_{c_i}^2)\pi_{c_i}}{\sum_k \mathcal{N}(\mathbf{z}_i|\mu_k, \sigma_k^2)\pi_k}, \quad (10)$$

while we define the variational distribution $q_{\phi}(\mathbf{z}_i|\mathbf{x}_i)$ to be a Gaussian distribution with mean $\mu_{\phi}(\mathbf{x}_i)$ and variance $\sigma_{\phi}^2(\mathbf{x}_i)$ parametrized by a neural network, also known as *encoder*.

2.4 Optimisation & Computational Complexity

The parameters of the generative model and the parameters of the variational distribution are optimised by maximising the C-ELBO. From Definitions 2 and 3, we derive Lemma 2:

Lemma 2. *The Conditional ELBO \mathcal{L}_C factorizes as follow:*

$$\begin{aligned} \mathcal{L}_C(\boldsymbol{\theta}, \boldsymbol{\phi}, \boldsymbol{\nu}, \boldsymbol{\pi}, \mathbf{X}|\mathbf{W}) = & -\log \Omega(\boldsymbol{\pi}) + \sum_{i=1}^N E_{q_\phi(\mathbf{z}_i|\mathbf{x}_i)} \left[\log p_\theta(\mathbf{x}_i|\mathbf{z}_i) - \log q_\phi(\mathbf{z}_i|\mathbf{x}_i) \right] \\ & + \sum_{i=1}^N E_{q_\phi(\mathbf{z}_i|\mathbf{x}_i)} \sum_{k=1}^K p(k|\mathbf{z}_i) \left[\log p(\mathbf{z}_i|k) + \log \pi_k - \log p(k|\mathbf{z}_i) \right] \quad (11) \\ & + \sum_{i \neq j=1}^N E_{q_\phi(\mathbf{z}_i|\mathbf{x}_i)} E_{q_\phi(\mathbf{z}_j|\mathbf{x}_j)} \sum_{k=1}^K p(k|\mathbf{z}_i) p(k|\mathbf{z}_j) \mathbf{W}_{i,j}, \end{aligned}$$

where $p(k|\mathbf{z}_i) = p(c_i = k|\mathbf{z}_i; \boldsymbol{\nu}, \boldsymbol{\pi})$ and $p(\mathbf{z}_i|k) = p(\mathbf{z}_i|c_i = k; \boldsymbol{\nu})$.

For the complete proof we refer to the Appendix B. Maximizing Eq. 11 w.r.t. $\boldsymbol{\pi}$ poses computational problems due to the normalization factor $\Omega(\boldsymbol{\pi})$. Crude approximations are investigated in (Basu et al., 2008), however we choose to fix the parameter $\pi_k = 1/K$ to make \mathbf{z} uniformly distributed in the latent space, as in previous works (Dilokthanakul et al., 2016). Hence the normalization factor can be treated as a constant. The Conditional ELBO can then be approximated using the SGVB estimator and the reparameterization trick (Kingma & Welling, 2014) to be trained efficiently using stochastic gradient descent. We refer to the Appendix B for the full derivation. We observe that the pairwise prior information only affects the last term, which scans through the dataset twice. To allow for fast iteration we simplify it by allowing the search of pairwise constraints to be performed only inside the considered batch, yielding

$$\frac{1}{L} \sum_{l=1}^L \sum_{i \neq j=1}^B \sum_{k=1}^K p(c_i = k|\mathbf{z}_i^{(l)}) p(c_j = k|\mathbf{z}_j^{(l)}) \mathbf{W}_{i,j}, \quad (12)$$

where L denotes the number of Monte Carlo samples and B the batch size. By doing so, the overhead in computational complexity of a single joint update of the parameters is $O(LB^2KC_p^2)$, where C_p is the cost of evaluating $p(c_i = k|\mathbf{z}_i)$ with $\mathbf{z}_i \in \mathbb{R}^D$. The latter is $O(KD)$.

3 Related Work

Constrained Clustering. A constrained clustering problem differs from the classical clustering scenario as the user has access to some pre-existing knowledge about the desired partition of the data expressed as instance-level constraints (Lange et al., 2005). Traditional clustering methods, such as the well-known K-means algorithm, have been extended to enforce pairwise constraints (Wagstaff et al. (2001), Bilenko et al. (2004)). Several methods also proposed a constrained version of the Gaussian Mixture Models (Shental et al., 2003; Law et al., 2004, 2005). Among them, penalized probabilistic clustering (PPC, Lu & Leen (2004)) is the most related to our work as it expresses the pairwise constraints as Bayesian priors over the assignment of data points to clusters, similarly to our model. However, all previous mentioned models shows poor performance and high computational complexity on high-dimensional and large-scale data sets.

Constrained Deep Clustering. To overcome the limitations of the above models, constrained clustering algorithms have lately been used in combination with deep neural networks (DNNs). Hsu & Kira (2015) train a DNN to minimize the Kullback-Leibler (KL) divergence between similar pairs of samples, while Chen (2015) performs semi-supervised maximum margin clustering on the learned features of a DNN. More recently, many extensions of the widely used DEC model (Xie et al., 2016) have been proposed to include a variety of loss functions to enforce pairwise constraints. Among them, SDEC, (Ren et al., 2019) includes a distance loss function that forces the data points with a must-link to be close in the latent space and vice-versa. Constrained IDEC (Zhang et al., 2019), uses a KL divergence loss instead, extending the work of Shukla et al. (2018). Smieja et al. (2020) focuses on discriminative clustering methods by self-generating pairwise constraints from Siamese networks.

As none of these approaches are based on generative models, the above methods fail to uncover the underlying data distribution.

Deep Generative Models. Although a wide variety of generative models have been proposed in the literature to perform unsupervised clustering (Li et al., 2019; Yang et al., 2019; Manduchi et al., 2019; Jiang et al., 2017), not much effort has been directed towards extending them to incorporate domain knowledge and clustering preferences. Nevertheless, the inclusion of prior information on a growing amount of unlabelled data is of profound practical importance in a wide range of applications (Kingma et al., 2014). The only exception is the work of Luo et al. (2018), where the authors proposed the SDCD algorithm, which has remarkably lower clustering performance compared to state-of-the-art constrained clustering models, as we will show in the experiments. Different from our approach, SDCD models the joint distribution of data and pairwise constraints. The authors adopt the two-coin Dawid-Skene model from Raykar et al. (2010) to model $p(\mathbf{W}|\mathbf{c})$, resulting in a different graphical model (see Fig. 1). Instead, we consider a simpler and more intuitive scenario, where we assume the cluster assignments are conditioned on the prior information, $p(\mathbf{c}|\mathbf{W}; \boldsymbol{\pi})$ (see Definition 2). In other words, we assume that different clustering structures might be present within a data set. The domain knowledge should then indicate which one is preferred over the other.

Table 1: Clustering performances (%) of our proposed method DC-GMM compared with baselines. All methods use 6000 pairwise constraints except the unsupervised VaDE and the SCDC. Means and standard deviations are computed across 10 runs with different random model initialization. *VaDE results are different from (Jiang et al., 2017) as they only report their best performance. **Results taken from (Luo et al., 2018).

Dataset	Metric	VaDE*	PCKmeans	SDEC	C-IDEDEC	SCDC**	DC-GMM (ours)
MNIST	Acc	89.0 \pm 5.0	56.4 \pm 2.0	86.2 \pm 0.1	96.3 \pm 0.2	84.2	96.6 \pm 0.1
	NMI	82.8 \pm 3.0	50.5 \pm 1.3	84.2 \pm 0.1	91.8 \pm 1.0	81.2	91.5 \pm 0.2
	ARI	80.9 \pm 5.0	38.8 \pm 1.9	80.1 \pm 0.1	92.1 \pm 0.4	-	92.7 \pm 0.3
FASHION	Acc	55.1 \pm 2.2	53.9 \pm 2.9	54.0 \pm 0.2	68.1 \pm 3.0	-	80.0 \pm 1.0
	NMI	57.9 \pm 2.7	50.8 \pm 1.3	57.3 \pm 0.1	66.7 \pm 2.0	-	71.8 \pm 0.5
	ARI	41.6 \pm 3.1	36.1 \pm 1.7	40.2 \pm 0.1	52.3 \pm 3.0	-	65.8 \pm 0.7
REUTERS	Acc	76.0 \pm 0.7	71.5 \pm 2.4	82.1 \pm 0.1	94.7 \pm 0.6	-	95.4 \pm 0.2
	NMI	50.1 \pm 1.3	48.2 \pm 3.8	62.3 \pm 0.1	81.4 \pm 0.7	-	82.7 \pm 0.7
	ARI	58.0 \pm 1.4	46.5 \pm 4.2	66.7 \pm 0.1	87.7 \pm 0.9	-	89.0 \pm 0.6
STL-10	Acc	77.3 \pm 0.5	70.3 \pm 4.2	79.2 \pm 0.1	81.6 \pm 3.8	-	89.5 \pm 0.5
	NMI	70.6 \pm 0.4	71.6 \pm 1.3	78.6 \pm 0.1	77.3 \pm 1.7	-	80.2 \pm 0.7
	ARI	62.7 \pm 0.4	58.4 \pm 2.1	71.0 \pm 0.1	71.8 \pm 3.4	-	78.4 \pm 0.9

4 Experiments

In the following, we provide a thorough empirical assessment of our proposed method (DC-GMM) with pairwise constraints using a wide range of data sets. First, we evaluate our model’s performance compared to both the unsupervised variational deep clustering method and state-of-the-art constrained clustering methods. As a next step, we present extensive evidence of the ability of our model to handle noisy constraint information. Additionally, we perform experiments on a challenging real medical data set consisting of pediatric heart ultrasound videos, as well as a face image data set to demonstrate that our model can reach different desirable partitions of the data, depending on the constraints used, with real-world, noisy data.

Baselines & Implementation Details. As baselines, we include the traditional pairwise constrained K-means (PCKmeans, Basu et al. (2004)) and two recent deterministic deep constrained clustering methods based on DEC (SDEC, Ren et al. (2019), and Constrained IDEC, Zhang et al. (2019)) as they achieve state-of-the-art performance in constrained clustering. For simplicity, we will refer to the latter as C-IDEDEC. We also compare our method to generative models, the semi-supervised SCDC (Luo et al., 2018) and the unsupervised VaDE (Jiang et al., 2017). To implement our model, we

were careful in maintaining a fair comparison with the baselines. In particular, we adopted the same encoder and decoder feed-forward architecture used by the baselines: four layers of 500, 500, 2000, D units respectively, where $D = 10$ unless stated otherwise. The VAE is pretrained for 10 epochs while the DEC-based baselines need a more complex layer-wise pretraining of the autoencoder which involves 50 epochs of pretraining for each layer and 100 epochs of pretraining as finetuning. Each data set is divided into training and test sets, and all the reported results are computed on the latter. We employed the same hyper-parameters for all data sets, see Appendix F.1 for details. The pairwise constraints are chosen randomly within the training set by sampling two data points and assigning a must-link if they have the same label and a cannot-link otherwise. Unless stated otherwise, the values of $|W_{i,j}|$ are set to 10^4 for all data sets, and 6000 pairwise constraints are used for both our model and the constrained clustering baselines. Note that the total amount of pairwise annotations in a data set of length N is $O(N^2)$. Given that N is typically larger than 10000, the number of pairwise constraints used in the experiments represents a small fraction of the total information.

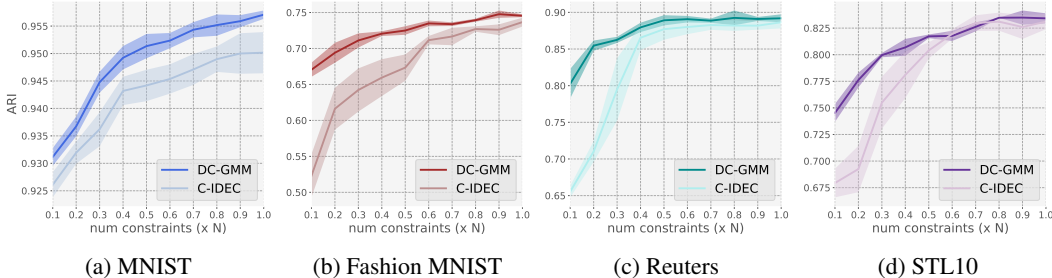


Figure 2: Comparison of clustering performance of our proposed DC-GMM model and the strongest baseline C-IDEC on four different data sets. The number of constraints vary between $0.1 \times N$ and N , where N is the length of the data set. ARI is used as evaluation metric.

Constrained clustering. We first compare the clustering performance of our model with the baselines on four different standard data sets: MNIST (LeCun et al., 2010), Fashion MNIST (Xiao et al., 2017), Reuters (Xie et al., 2016) and STL-10 (Coates et al., 2011) (see Appendix A). More complex data sets will be explored in the following paragraphs. Note that we pre-processed the Reuters data by computing the tf-idf features on the 2000 most frequent words on a random subset of 10 000 documents and by selecting 4 root categories (Xie et al., 2016). Additionally, we extracted features from the STL-10 image data set using a ResNet-50 (He et al., 2016), as in previous works (Jiang et al., 2017). Accuracy, Normalized Mutual Information (NMI), and Adjusted Rand Index (ARI) are used as evaluation metrics. In Table 1 we report the mean and standard deviation of the clustering performance across 10 runs of both our method and the baselines. The only exception is the SDCD, for which we only report their original results (Luo et al., 2018) computed with a higher number of constraints. The provided code with 6000 constraints produced highly unstable and sub-optimal results (see Appendix D).

We observe that our model reaches state-of-the-art clustering performance in almost all metrics and data sets. As C-IDEC turns out to be the strongest baseline, we performed additional comparison to investigate the difference in performance under different settings. In Figure 2 we plot the clustering performance in terms of ARI using a varying number of constraints, N_c . For additional metrics, we refer to the Appendix E.1. We observe that our method outperforms the strongest baseline C-IDEC by a large margin on all four data sets when fewer constraints are used. When N_c gets close to N , the two methods tend to saturate on the Reuters and STL data sets.

Constrained clustering with noisy labels. In real-world applications it is often the case that the additional information comes from different sources with different confidence levels. Hence, the ability to integrate constraints with different degrees of certainty into the clustering algorithm is of significant practical importance. In this experiment, we consider the case in which the given pairwise constraints have three different noise levels, $q \in \{0.1, 0.2, 0.3\}$, where q determines the fraction of pairwise constraints with flipped signs (that is, when a must-link is turned into a cannot-link and vice-versa). In Fig. 3 we show the ARI clustering performance of our model compared to the strongest baseline derived from the previous section, C-IDEC. For all data sets, we decrease the value of the pairwise confidence of our method using the heuristic $|W_{i,j}| = \alpha \log \left(\frac{1-q}{q} \right)$ with $\alpha = 1000$.

Also, we use grid search to choose the hyper-parameters of C-IDEC for the different noise levels (in particular we set the penalty weight of their loss function to 0.01, 0.005, and 0.001 respectively). Additionally, we report Accuracy and NMI in Appendix E.2. DC-GMM clearly achieves better performance on all three noise levels for all data sets. In particular, the higher the noise level, the greater the difference in performance. We conclude that our model is more robust than its main competitor on noisy labels and it can easily include different sources of information with different degrees of uncertainty.

Heart Echo. We evaluate the capability of our model in a real-world application by using a data set consisting of 305 infant echo cardiogram videos obtained from the Hospital Barmherzige Brüder Regensburg. The videos are taken from five different angles (called views), denoted by [LA, KAKL, KAPAP, KAAP, 4CV]. Preprocessing of the data includes cropping the videos, resizing them to 64×64 pixels and splitting them into a total of 20000 individual frames. We investigated two different constrained clustering settings. First, we cluster the echo video frames by view (Zhang et al., 2018). Then, we cluster the echo video frames by infant maturity at birth, following the WHO definition of premature birth categories ("Preterm"). We believe that these two clustering tasks demonstrate that our model admits a degree of control in choosing the underlying structure of the learned clusters. For both experiments, we compare the performance of our method with the unsupervised VaDE and with C-IDEC. Additionally, we include a variant of both our method and VaDE in which we use a VGG-like convolutional neural network (Simonyan & Zisserman, 2015), for details on the implementation we refer to the Appendix F.2. The results are shown in Table 2. The DC-GMM outperforms both baselines by a significant margin in accuracy, NMI, and ARI, as well as in both clustering experiments. We also observe that C-IDEC performs poorly on real-world noisy data. We believe this is due to the heavy pretraining of the autoencoder, required by DEC-based methods, as it does not always lead to a learned latent space that is suitable for the clustering task. Additionally, we illustrate a PCA decomposition of the embedded space learned by both the DC-GMM and the unsupervised VaDE baseline for both tasks in Figure 4. Our method is clearly able to learn an embedded space that clusters both the different views and the different preterms more effectively than the unsupervised VaDE. This observation, together with the quantitative results, demonstrates that adding domain knowledge is particularly effective for medical purposes.

Face Images. We further evaluate the performance of our model using the UTKFace data set (Zhang et al., 2017). This data set contains over 20000 images of male and female faces, aged from 1 to 118 years old, with multiple ethnicities represented. We use VGG nets (Simonyan & Zisserman, 2015) for the VAE (the implementation details are described in the Appendix F.3). As in the Heart Echo experiment, we chose two different clustering tasks. First we cluster the data using the gender prior information, then we select a sub-sample of individuals between 18 and 50 years of age (approx. 11000 samples) and cluster by ethnicity (White, Black, Indian, Asian). In Fig. 5 we illustrate the PCA decomposition of the embedded space learned by the VaDE and our model. For both tasks we use $2N$ pairwise constraints where N is the length of the data set, which requires labels for 1.5% of the entire data set. Specifically, on the gender task and the ethnicity task our model achieves an accuracy of 0.89 and 0.85, which outperforms VaDE with a relative increase ratio of 74.5% and 49.1%. In terms of NMI, the unsupervised VaDE performance is close to 0 in both tasks, while our model performance is 0.52 and 0.54 respectively. Visually, we observe a neat division of the selected

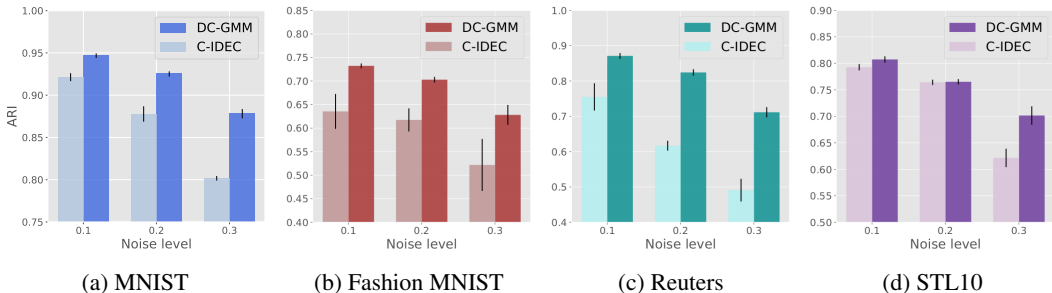


Figure 3: Comparison of clustering performance of our proposed DC-GMM model and the strongest baseline C-IDEC on four different data sets with noisy labels. ARI is used as evaluation metric.

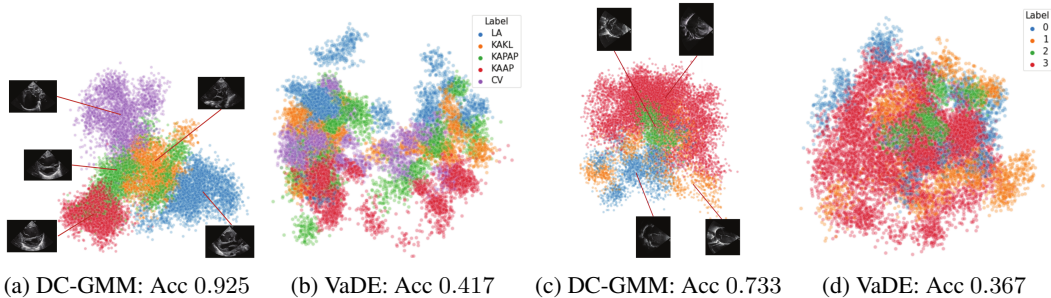


Figure 4: PCA decomposition of heart ultrasound imaging test set examples in the embedded space and generative samples using the unsupervised VaDE and our model DC-GMM with 6000 constraints for (a)-(b) View, (c)-(d) Preterm.

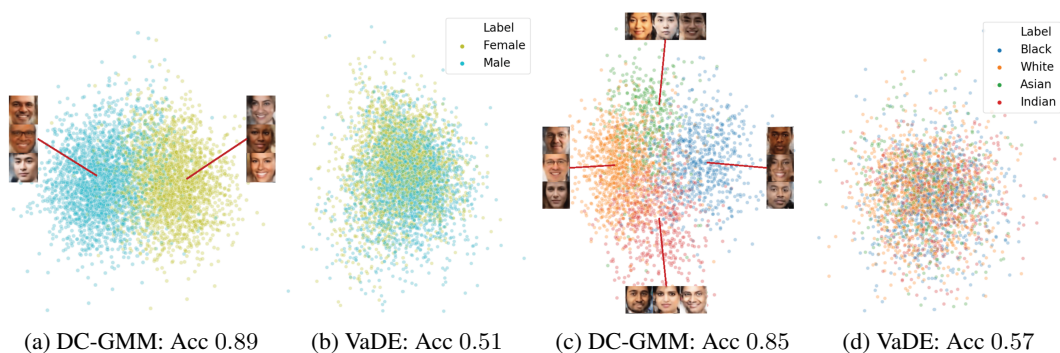


Figure 5: PCA decomposition of test set examples in the embedded space and generative samples using VaDE and DC-GMM for (a)-(b) Gender, (c)-(d) Ethnicity. In this configuration, DC-GMM obtains a NMI of 0.52 (gender) and 0.58 (ethnicity) while VaDE obtains a NMI close to 0 for both tasks.

clusters in the embedding space with the inclusion of domain knowledge. The unsupervised approach is not able to distinguish any feature of interest. We conclude that it is indeed possible to guide the clustering process towards a preferred configuration, depending on what the practitioners are seeking in the data, by providing different pairwise constraints. Finally, we tested the generative capabilities of our model by sampling from the learnt generative process of Sec 2.1. For a visualization of the generated sample we refer to the Appendix E.3.

Table 2: Clustering performance (%) using the heart echo cardiogram data with fully connected layers on the left and convolutional layers (CNN-) on the right. All methods use 6000 pairwise constraints except the VaDE. Means and standard deviations are computed across 10 runs with different random model initialization.

Clustering	Metric	VaDE	C-IDECE	DC-GMM	CNN-VaDE	CNN-DC-GMM
View	Acc	33.4 \pm 3.3	55.1 \pm 16.0	83.2 \pm 1.4	41.7 \pm 5.2	92.5 \pm 1.4
	NMI	8.9 \pm 2.7	33.3 \pm 15.9	64.9 \pm 2.3	19.7 \pm 7.4	82.6 \pm 3.0
	ARI	6.5 \pm 2.5	31.2 \pm 15.1	63.7 \pm 2.7	13.7 \pm 6.3	83.1 \pm 3.1
Preterm	Acc	41.4 \pm 5.4	69.6 \pm 1.1	72.3 \pm 1.5	36.7 \pm 2.5	73.3 \pm 1.1
	NMI	6.4 \pm 1.8	8.3 \pm 11.8	25.1 \pm 3.4	6.5 \pm 4.0	32.0 \pm 2.4
	ARI	2.3 \pm 2.6	13.7 \pm 19.3	45.1 \pm 4.1	3.9 \pm 3.8	48.1 \pm 2.8

5 Conclusion

In this work, we present a novel constrained deep clustering method called DC-GMM, that incorporates clustering preferences in the form of pairwise constraints, with varying degrees of certainty. In contrast to existing deep clustering approaches, DC-GMM uncovers the underlying distribution of the data conditioned on prior clustering preferences. With the integration of domain knowledge, we show that our model can drive the clustering algorithm towards the partitions of the data sought by the practitioners, achieving state-of-the-art constrained clustering performance in real-world and complex data sets. Additionally, our model proves to be robust to noisy constraints as it can efficiently include uncertainty into the clustering preferences. As a result, the proposed model can be applied to a variety of applications where the difficulty of obtaining labeled data prevents the use of fully supervised algorithms.

Limitations & Future Work The proposed algorithm requires that the mixing parameters π of the clusters are chosen *a priori*. This limitation is mitigated by the prior information \mathbf{W} , which permits a more flexible prior distribution if enough information is available (see Definition 2). The analysis of different approaches to learn the weights π represents a potential direction for future work. Additionally, the proposed framework could also be used in a self-supervised manner, by learning \mathbf{W} from the data using, e.g. contrastive learning approaches (Chen et al., 2020; Wu et al., 2018).

6 Code and Data Availability

The code is available in a GitHub repository: <https://github.com/lauramanduchi/DC-GMM>. All datasets are publicly available except the Heart Echo data. The latter is not available due to medical confidentiality.

References

- Basu, S., Banerjee, A., and Mooney, R. Active semi-supervision for pairwise constrained clustering. In *SDM*, 2004.
- Basu, S., Davidson, I., and Wagstaff, K. Constrained clustering: Advances in algorithms, theory, and applications. 2008.
- Bilenko, M., Basu, S., and Mooney, R. Integrating constraints and metric learning in semi-supervised clustering. In *ICML '04*, 2004.
- Blatt, M., Wiseman, S., and Domany, E. Superparamagnetic clustering of data. *Phys. Rev. Lett.*, 76: 3251–3254, Apr 1996. doi: 10.1103/PhysRevLett.76.3251. URL <https://link.aps.org/doi/10.1103/PhysRevLett.76.3251>.
- Chen, G. Deep transductive semi-supervised maximum margin clustering. *ArXiv*, abs/1501.06237, 2015.
- Chen, T., Kornblith, S., Norouzi, M., and Hinton, G. E. A simple framework for contrastive learning of visual representations. *ArXiv*, abs/2002.05709, 2020.
- Coates, A., Ng, A., and Lee, H. An analysis of single-layer networks in unsupervised feature learning. In *AISTATS*, 2011.
- Dilokthanakul, N., Mediano, P. A. M., Garnelo, M., Lee, M. C. H., Salimbeni, H., Arulkumaran, K., and Shanahan, M. Deep unsupervised clustering with gaussian mixture variational autoencoders. *ArXiv*, abs/1611.02648, 2016.
- He, K., Zhang, X., Ren, S., and Sun, J. Deep residual learning for image recognition. *2016 IEEE Conference on Computer Vision and Pattern Recognition (CVPR)*, pp. 770–778, 2016.
- Hsu, Y.-C. and Kira, Z. Neural network-based clustering using pairwise constraints. *ArXiv*, abs/1511.06321, 2015.

- Jiang, Z., Zheng, Y., Tan, H., Tang, B., and Zhou, H. Variational deep embedding: An unsupervised and generative approach to clustering. In *IJCAI*, 2017.
- Kingma, D. P. and Welling, M. Auto-encoding variational bayes. In Bengio, Y. and LeCun, Y. (eds.), *2nd International Conference on Learning Representations, ICLR 2014, Banff, AB, Canada, April 14-16, 2014, Conference Track Proceedings*, 2014. URL <http://arxiv.org/abs/1312.6114>.
- Kingma, D. P., Mohamed, S., Rezende, D. J., and Welling, M. Semi-supervised learning with deep generative models. In *NIPS*, 2014.
- Lange, T., Law, M. H. C., Jain, A. K., and Buhmann, J. Learning with constrained and unlabelled data. *2005 IEEE Computer Society Conference on Computer Vision and Pattern Recognition (CVPR'05)*, 1:731–738 vol. 1, 2005.
- Law, M. H. C., Topchy, A., and Jain, A. K. Clustering with soft and group constraints. In *SSPR/SPR*, 2004.
- Law, M. H. C., Topchy, A., and Jain, A. K. Model-based clustering with probabilistic constraints. In *SDM*, 2005.
- LeCun, Y., Cortes, C., and Burges, C. Mnist handwritten digit database. *ATT Labs [Online]*. Available: <http://yann.lecun.com/exdb/mnist>, 2, 2010.
- Lewis, D. D., Yang, Y., Rose, T. G., and Li, F. Rcv1: A new benchmark collection for text categorization research. *J. Mach. Learn. Res.*, 5:361–397, December 2004. ISSN 1532-4435.
- Li, X., Chen, Z., Poon, L. K. M., and Zhang, N. L. Learning latent superstructures in variational autoencoders for deep multidimensional clustering. In *ICLR*, 2019.
- Lu, Z. and Leen, T. Semi-supervised learning with penalized probabilistic clustering. In *NIPS*, 2004.
- Luo, Y., TIAN, T., Shi, J., Zhu, J., and Zhang, B. Semi-crowdsourced clustering with deep generative models. In Bengio, S., Wallach, H., Larochelle, H., Grauman, K., Cesa-Bianchi, N., and Garnett, R. (eds.), *Advances in Neural Information Processing Systems 31*, pp. 3212–3222. Curran Associates, Inc., 2018.
- Manduchi, L., Hüser, M., Rätsch, G., and Fortuin, V. Variational psom: Deep probabilistic clustering with self-organizing maps. *ArXiv*, abs/1910.01590, 2019.
- Min, E., Guo, X., Liu, Q., Zhang, G., Cui, J., and Long, J. A survey of clustering with deep learning: From the perspective of network architecture. *IEEE Access*, 6:39501–39514, 2018.
- Raykar, V. C., Yu, S., Zhao, L. H., Valadez, G. H., Florin, C., Bogoni, L., and Moy, L. Learning from crowds. *Journal of Machine Learning Research*, 11(43):1297–1322, 2010. URL <http://jmlr.org/papers/v11/raykar10a.html>.
- Ren, Y., Hu, K., Dai, X., Pan, L., Hoi, S. C. H., and Xu, Z. Semi-supervised deep embedded clustering. *Neurocomputing*, 325:121–130, 2019.
- Rezende, D. J., Mohamed, S., and Wierstra, D. Stochastic backpropagation and approximate inference in deep generative models. In *ICML*, 2014.
- Shental, N., Bar-Hillel, A., Hertz, T., and Weinshall, D. Computing gaussian mixture models with em using equivalence constraints. In *NIPS*, 2003.
- Shukla, A., Cheema, G. S., and Anand, S. Semi-supervised clustering with neural networks. *arXiv: Learning*, 2018.
- Simonyan, K. and Zisserman, A. Very deep convolutional networks for large-scale image recognition. *CoRR*, abs/1409.1556, 2015.
- Smieja, M., Struski, L., and Figueiredo, M. A. T. A classification-based approach to semi-supervised clustering with pairwise constraints. *Neural networks : the official journal of the International Neural Network Society*, 127:193–203, 2020.

- Wagstaff, K. and Cardie, C. Clustering with instance-level constraints. In *AAAI/IAAI*, 2000.
- Wagstaff, K., Cardie, C., Rogers, S., and Schrödl, S. Constrained k-means clustering with background knowledge. In *ICML*, 2001.
- Wu, F. Y. The potts model. *Rev. Mod. Phys.*, 54:235–268, Jan 1982. doi: 10.1103/RevModPhys.54.235. URL <https://link.aps.org/doi/10.1103/RevModPhys.54.235>.
- Wu, Z., Xiong, Y., Yu, S., and Lin, D. Unsupervised feature learning via non-parametric instance discrimination. *2018 IEEE/CVF Conference on Computer Vision and Pattern Recognition*, pp. 3733–3742, 2018.
- Xiao, H., Rasul, K., and Vollgraf, R. Fashion-mnist: a novel image dataset for benchmarking machine learning algorithms, 2017.
- Xie, J., Girshick, R., and Farhadi, A. Unsupervised deep embedding for clustering analysis. volume 48 of *Proceedings of Machine Learning Research*, pp. 478–487, New York, New York, USA, 20–22 Jun 2016. PMLR. URL <http://proceedings.mlr.press/v48/xieb16.html>.
- Yang, L., Cheung, N., Li, J., and Fang, J. Deep clustering by gaussian mixture variational autoencoders with graph embedding. *2019 IEEE/CVF International Conference on Computer Vision (ICCV)*, pp. 6439–6448, 2019.
- Zhang, H., Basu, S., and Davidson, I. A framework for deep constrained clustering - algorithms and advances. In *ECML/PKDD*, 2019.
- Zhang, J., Gajjala, S., Agrawal, P., Tison, G., Hallock, L., Beussink, L., Lassen, M., Fan, E., Aras, M., Jordan, C., Fleischmann, K., Melisko, M., Qasim, A., Shah, S., Bajcsy, R., and Deo, R. Fully automated echocardiogram interpretation in clinical practice: Feasibility and diagnostic accuracy. *Circulation*, 138:1623–1635, 10 2018. doi: 10.1161/CIRCULATIONAHA.118.034338.
- Zhang, Z., Song, Y., and Qi, H. Age progression/regression by conditional adversarial autoencoder. *2017 IEEE Conference on Computer Vision and Pattern Recognition (CVPR)*, pp. 4352–4360, 2017.

Appendix

A Data sets

The data sets used in the experiments are the followings:

- **MNIST:** It consists of 70 000 handwritten digits. The images are centered and of size 28 by 28 pixels. We reshaped each image to a 784-dimensional vector (LeCun et al., 2010).
- **Fashion MNIST:** A data set of Zalando’s article images consisting of a training set of 60 000 examples and a test set of 10 000 examples (Xiao et al., 2017).
- **Reuters:** It contains 810 000 English news stories (Lewis et al., 2004). Following the work of Xie et al. (2016), we used 4 root categories: corporate/industrial, government/social, markets, and economics as labels and discarded all documents with multiple labels, which results in a 685 071-article data set. We computed tf-idf features on the 2000 most frequent words to represent all articles. A random subset of 10 000 documents is then sampled.
- **STL10:** It contains color images of 96-by-96 pixel size. There are 10 classes with 13 000 examples each (Coates et al., 2011). As pre-processing, we extracted features from the STL-10 image data set using a ResNet-50 (He et al., 2016), as in previous works (Jiang et al., 2017).
- **Newborn echo cardiograms:** The data set consists of 305 infant echo cardiogram videos from the Hospital Barmherzige Brüder Regensburg. The videos are taken from several different angles, denoted by [LA, KAKL, KAPAP, KAAP, 4CV]. We cropped the videos by isolating the cone of the echo cardiogram, we resized them to 64x64 pixels and split them into individual frames obtaining a total of $N = 20000$ images. The data used is highly sensitive patient data, hence we only use data with informed consent available. Approval for reuse of the data for our research was obtained from the responsible Ethics Committees. In addition, all data is pseudonymized.
- **UTKFace:** This data set contains over 20 000 images of male and female face of individuals from 1 to 118 years old, with multiple ethnicities represented (Zhang et al., 2017).

B Conditional ELBO Derivations

B.1 Proof of Lemma 1

1. The C-ELBO \mathcal{L}_C is a lower bound of the marginal log-likelihood conditioned on \mathbf{W} , that is

$$\log p(\mathbf{X}|\mathbf{W}) \geq \mathcal{L}_C(\boldsymbol{\theta}, \boldsymbol{\phi}, \boldsymbol{\nu}, \boldsymbol{\pi}, \mathbf{X}|\mathbf{W}).$$

2. $\log p(\mathbf{X}|\mathbf{W}) = \mathcal{L}_C(\boldsymbol{\theta}, \boldsymbol{\phi}, \boldsymbol{\nu}, \boldsymbol{\pi}, \mathbf{X}|\mathbf{W})$ if and only if $q_\phi(\mathbf{Z}, \mathbf{c}|\mathbf{X}) = p(\mathbf{Z}, \mathbf{c}|\mathbf{X}, \mathbf{W})$.

Proof. The marginal log-likelihood conditioned on \mathbf{W} can be written as

$$\log p(\mathbf{X}|\mathbf{W}) = \mathbb{E}_{q_\phi(\mathbf{Z}, \mathbf{c}|\mathbf{X})} \log p(\mathbf{X}|\mathbf{W}) \quad (13)$$

$$= \mathbb{E}_{q_\phi(\mathbf{Z}, \mathbf{c}|\mathbf{X})} \left[\log \frac{p(\mathbf{X}, \mathbf{Z}, \mathbf{c}|\mathbf{W})}{p(\mathbf{Z}, \mathbf{c}|\mathbf{X}, \mathbf{W})} + q_\phi(\mathbf{Z}, \mathbf{c}|\mathbf{X}) - q_\phi(\mathbf{Z}, \mathbf{c}|\mathbf{X}) \right] \quad (14)$$

$$= \mathbb{E}_{q_\phi(\mathbf{Z}, \mathbf{c}|\mathbf{X})} \log \frac{p(\mathbf{X}, \mathbf{Z}, \mathbf{c}|\mathbf{W})}{q_\phi(\mathbf{Z}, \mathbf{c}|\mathbf{X})} + \mathbb{E}_{q_\phi(\mathbf{Z}, \mathbf{c}|\mathbf{X})} \log \frac{q_\phi(\mathbf{Z}, \mathbf{c}|\mathbf{X})}{p(\mathbf{Z}, \mathbf{c}|\mathbf{X}, \mathbf{W})}. \quad (15)$$

The first term corresponds to the C-ELBO. We prove this by using Definition 3 and Eq. 7:

$$\mathbb{E}_{q_\phi(\mathbf{Z}, \mathbf{c}|\mathbf{X})} \log \frac{p(\mathbf{X}, \mathbf{Z}, \mathbf{c}|\mathbf{W})}{q_\phi(\mathbf{Z}, \mathbf{c}|\mathbf{X})} = \mathbb{E}_{q_\phi(\mathbf{Z}, \mathbf{c}|\mathbf{X})} \log \frac{p_\theta(\mathbf{X}|\mathbf{Z})p(\mathbf{Z}, \mathbf{c}|\mathbf{W}; \boldsymbol{\nu}, \boldsymbol{\pi})}{q_\phi(\mathbf{Z}, \mathbf{c}|\mathbf{X})} \quad (16)$$

$$= \mathbb{E}_{q_\phi(\mathbf{Z}, \mathbf{c}|\mathbf{X})} [\log p_\theta(\mathbf{X}|\mathbf{Z})] + \mathbb{E}_{q_\phi(\mathbf{Z}, \mathbf{c}|\mathbf{X})} \left[\log \frac{p(\mathbf{Z}, \mathbf{c}|\mathbf{W}; \boldsymbol{\nu}, \boldsymbol{\pi})}{q_\phi(\mathbf{Z}, \mathbf{c}|\mathbf{X})} \right] \quad (17)$$

$$= \mathbb{E}_{q_\phi(\mathbf{Z}|\mathbf{X})} [\log p_\theta(\mathbf{X}|\mathbf{Z})] - D_{KL}(q_\phi(\mathbf{Z}, \mathbf{c}|\mathbf{X}) \| p(\mathbf{Z}, \mathbf{c}|\mathbf{W}; \boldsymbol{\nu}, \boldsymbol{\pi})) \quad (18)$$

$$= \mathcal{L}_C(\boldsymbol{\theta}, \boldsymbol{\phi}, \boldsymbol{\nu}, \boldsymbol{\pi}, \mathbf{X}|\mathbf{W}). \quad (19)$$

Combining Eq. 15 with Eq. 19, the following holds:

$$\log p(\mathbf{X}|\mathbf{W}) = \mathcal{L}_C(\boldsymbol{\theta}, \boldsymbol{\phi}, \boldsymbol{\nu}, \boldsymbol{\pi}, \mathbf{X}|\mathbf{W}) + D_{KL}(q_\phi(\mathbf{Z}, \mathbf{c}|\mathbf{X})\|p(\mathbf{Z}, \mathbf{c}|\mathbf{X}, \mathbf{W})). \quad (20)$$

Given the non-negativity of the Kullback–Leibler divergence, that is $D_{KL}(q\|p) \geq 0$, it follows that $\log p(\mathbf{X}|\mathbf{W}) \geq \mathcal{L}_C(\boldsymbol{\theta}, \boldsymbol{\phi}, \boldsymbol{\nu}, \boldsymbol{\pi}, \mathbf{X}|\mathbf{W})$. Finally, given that $D_{KL}(q\|p) = 0$ if and only if $q(\cdot) = p(\cdot)$ the second part of the Lemma follows. \square

B.2 Proof of Lemma 2

The Conditional ELBO \mathcal{L}_C factorizes as follow:

$$\begin{aligned} \mathcal{L}_C(\boldsymbol{\theta}, \boldsymbol{\phi}, \boldsymbol{\nu}, \boldsymbol{\pi}, \mathbf{X}|\mathbf{W}) &= -\log \Omega(\boldsymbol{\pi}) + \sum_{i=1}^N E_{q_\phi(\mathbf{z}_i|\mathbf{x}_i)} \left[\log p_\theta(\mathbf{x}_i|\mathbf{z}_i) - \log q_\phi(\mathbf{z}_i|\mathbf{x}_i) \right] \\ &+ \sum_{i=1}^N E_{q_\phi(\mathbf{z}_i|\mathbf{x}_i)} \sum_{k=1}^K p(k|\mathbf{z}_i) \left[\log p(\mathbf{z}_i|k) + \log \pi_k - \log p(k|\mathbf{z}_i) \right] \quad (21) \\ &+ \sum_{i \neq j=1}^N E_{q_\phi(\mathbf{z}_i|\mathbf{x}_i)} E_{q_\phi(\mathbf{z}_j|\mathbf{x}_j)} \sum_{k=1}^K p(k|\mathbf{z}_i) p(k|\mathbf{z}_j) \mathbf{W}_{i,j}, \end{aligned}$$

where $p(k|\mathbf{z}_i) = p(c_i = k|\mathbf{z}_i; \boldsymbol{\nu}, \boldsymbol{\pi})$ and $p(\mathbf{z}_i|k) = p(\mathbf{z}_i|c_i = k; \boldsymbol{\nu})$.

Proof. Using Definition 3 and Eq. 7, the Conditional ELBO can be further factorized as:

$$\begin{aligned} \mathcal{L}_C(\boldsymbol{\theta}, \boldsymbol{\phi}, \boldsymbol{\nu}, \boldsymbol{\pi}, \mathbf{X}|\mathbf{W}) &= E_{q_\phi(\mathbf{Z}|\mathbf{X})} [\log p_\theta(\mathbf{X}|\mathbf{Z})] + E_{q_\phi(\mathbf{Z}, \mathbf{c}|\mathbf{X})} [\log p(\mathbf{Z}|\mathbf{c}; \boldsymbol{\nu})] \\ &+ E_{q_\phi(\mathbf{Z}, \mathbf{c}|\mathbf{X})} [\log p(\mathbf{c}|\mathbf{W}; \boldsymbol{\pi})] - E_{q_\phi(\mathbf{Z}, \mathbf{c}|\mathbf{X})} [\log q_\phi(\mathbf{Z}, \mathbf{c}|\mathbf{X})]. \quad (22) \end{aligned}$$

By plugging in the variational distribution of Eq. 9, the C-ELBO reads:

$$\begin{aligned} \mathcal{L}_C(\boldsymbol{\theta}, \boldsymbol{\phi}, \boldsymbol{\nu}, \boldsymbol{\pi}, \mathbf{X}|\mathbf{W}) &= \mathbb{E}_{q_\phi(\mathbf{Z}|\mathbf{X})} [\log p_\theta(\mathbf{X}|\mathbf{Z})] + \mathbb{E}_{q_\phi(\mathbf{Z}|\mathbf{X}) p(\mathbf{c}|\mathbf{Z}; \boldsymbol{\nu}, \boldsymbol{\pi})} [\log p(\mathbf{Z}|\mathbf{c}; \boldsymbol{\nu})] \\ &+ \mathbb{E}_{q_\phi(\mathbf{Z}|\mathbf{X}) p(\mathbf{c}|\mathbf{Z}; \boldsymbol{\nu}, \boldsymbol{\pi})} [\log p(\mathbf{c}|\mathbf{W}; \boldsymbol{\pi})] - \mathbb{E}_{q_\phi(\mathbf{Z}|\mathbf{X})} [\log q_\phi(\mathbf{Z}|\mathbf{X})] \quad (23) \\ &- \mathbb{E}_{q_\phi(\mathbf{Z}|\mathbf{X}) p(\mathbf{c}|\mathbf{Z}; \boldsymbol{\nu}, \boldsymbol{\pi})} [\log p(\mathbf{c}|\mathbf{Z}; \boldsymbol{\nu}, \boldsymbol{\pi})]. \end{aligned}$$

The third term depends on \mathbf{W} and is investigated in the following. Given that $q_\phi(\mathbf{Z}|\mathbf{X}) p(\mathbf{c}|\mathbf{Z}) = \prod_i q_\phi(\mathbf{z}_i|\mathbf{x}_i) p(c_i|\mathbf{z}_i)$ and using Definition 2, $E_{q_\phi(\mathbf{Z}, \mathbf{c}|\mathbf{X})} [\log p(\mathbf{c}|\mathbf{W})]$ can be factorized as

$$E_{q_\phi(\mathbf{Z}, \mathbf{c}|\mathbf{X})} [\log p(\mathbf{c}|\mathbf{W})] = E_{q_\phi(\mathbf{Z}, \mathbf{c}|\mathbf{X})} \log \frac{1}{\Omega(\boldsymbol{\pi})} \prod_i \pi_{c_i} \prod_{j \neq i} \exp(\mathbf{W}_{i,j} \delta_{c_i c_j}) \quad (24)$$

$$= -\log \Omega(\boldsymbol{\pi}) + \sum_{i=1}^N E_{q_\phi(\mathbf{z}_i, c_i|\mathbf{x}_i)} \log \pi_{c_i} + \sum_{i,j=1, i \neq j}^N E_{q_\phi(\mathbf{z}_i, c_i|\mathbf{x}_i)} E_{q_\phi(\mathbf{z}_j, c_j|\mathbf{x}_j)} \mathbf{W}_{i,j} \delta_{c_i c_j}, \quad (25)$$

By observing that $E_{q_\phi(\mathbf{z}_i, c_i|\mathbf{x}_i)}(\cdot) = E_{q_\phi(\mathbf{z}_i|\mathbf{x}_i)} \sum_{k=1}^K p(c_i = k|\mathbf{z}_i; \boldsymbol{\nu}, \boldsymbol{\pi})(\cdot)$ the last term of Eq. 25 can be written as:

$$\sum_{i,j=1, i \neq j}^N E_{q_\phi(\mathbf{z}_i|\mathbf{x}_i)} E_{q_\phi(\mathbf{z}_j|\mathbf{x}_j)} \sum_{k=1}^K p(c_i = k|\mathbf{z}_i; \boldsymbol{\nu}, \boldsymbol{\pi}) \sum_{h=1}^K p(c_i = h|\mathbf{z}_j; \boldsymbol{\nu}, \boldsymbol{\pi}) \mathbf{W}_{i,j} \delta_{k,h} \quad (26)$$

$$= \sum_{i,j=1, i \neq j}^N E_{q_\phi(\mathbf{z}_i|\mathbf{x}_i)} E_{q_\phi(\mathbf{z}_j|\mathbf{x}_j)} \sum_{k=1}^K p(c_i = k|\mathbf{z}_i; \boldsymbol{\nu}, \boldsymbol{\pi}) p(c_i = k|\mathbf{z}_j; \boldsymbol{\nu}, \boldsymbol{\pi}) \mathbf{W}_{i,j} \quad (27)$$

Given the above equations, Eq. can be further factorized as

$$\begin{aligned}
\mathcal{L}_C(\mathbf{X}|\mathbf{G}) &= \sum_{i=1}^N \mathbb{E}_{q_\phi(\mathbf{z}_i|\mathbf{x}_i)} [\log p_\theta(\mathbf{x}_i|\mathbf{z}_i)] \\
&+ \sum_{i=1}^N \mathbb{E}_{q_\phi(\mathbf{z}_i|\mathbf{x}_i)} \left[\sum_{k=1}^K p(\mathbf{c}_i = k|\mathbf{z}_i) \log p(\mathbf{z}_i|\mathbf{c}_i = k) \right] \\
&- \log \Omega(\boldsymbol{\pi}) + \sum_{i=1}^N \mathbb{E}_{q_\phi(\mathbf{z}_i|\mathbf{x}_i)} \sum_{k=1}^K p(\mathbf{c}_i = k|\mathbf{z}_i) \log \pi_{\mathbf{c}_i} \\
&+ \sum_{i,j=1, i \neq j}^N \mathbb{E}_{q_\phi(\mathbf{z}_i|\mathbf{x}_i)} \mathbb{E}_{q_\phi(\mathbf{z}_j|\mathbf{x}_j)} \sum_{k=1}^K p(\mathbf{c}_i = k|\mathbf{z}_i) p(\mathbf{c}_j = k|\mathbf{z}_j) \mathbf{W}_{i,j} \\
&- \sum_{i=1}^N \mathbb{E}_{q_\phi(\mathbf{z}_i|\mathbf{x}_i)} [\log q(\mathbf{z}_i|\mathbf{x}_i)] \\
&- \sum_{i=1}^N \mathbb{E}_{q_\phi(\mathbf{z}_i|\mathbf{x}_i)} \sum_{k=1}^K p(\mathbf{c}_i = k|\mathbf{z}_i) [\log p(\mathbf{c}_i = k|\mathbf{z}_i)].
\end{aligned} \tag{28}$$

where we simplified $p(\mathbf{c}|\mathbf{z}_i; \boldsymbol{\nu}, \boldsymbol{\pi})$ in $p(\mathbf{c}|\mathbf{z}_i)$ for clarity. By re-ordering the terms the above equation is equal to Eq. 21. \square

B.3 Optimisation with the SGVB estimator

Using the SGVB estimator (Kingma & Welling, 2014; Rezende et al., 2014), we can approximate the C-ELBO defined in Eq. 11 as:

$$\begin{aligned}
\mathcal{L}_C(\mathbf{X}|\mathbf{G}) &= \sum_{i=1}^N \frac{1}{L} \sum_{l=1}^L \left[\log p_\theta(\mathbf{x}_i|\mathbf{z}_i^{(l)}) - \log q_\phi(\mathbf{z}_i^{(l)}|\mathbf{x}_i) \right. \\
&+ \sum_{k=1}^K p(\mathbf{c}_i = k|\mathbf{z}_i^{(l)}) \log p(\mathbf{z}_i^{(l)}|\mathbf{c}_i = k) + \sum_{k=1}^K p(\mathbf{c}_i = k|\mathbf{z}_i^{(l)}) \log \pi_{\mathbf{c}_i} \\
&- \left. \sum_{k=1}^K p(\mathbf{c}_i = k|\mathbf{z}_i^{(l)}) \log p(\mathbf{c}_i = k|\mathbf{z}_i^{(l)}) \right] \\
&+ \sum_{i,j=1, i \neq j}^N \sum_{k=1}^K p(\mathbf{c}_i = k|\mathbf{z}_i^{(l)}) p(\mathbf{c}_j = k|\mathbf{z}_j^{(l)}) \mathbf{W}_{i,j},
\end{aligned} \tag{29}$$

where $\log \Omega(\boldsymbol{\pi})$ is treated as constant and removed from the objective, L is the number of Monte Carlo samples in the SGVB estimator and it is set to $L = 1$ in all experiments.

C Further possible Constraints

Given the flexibility of our general framework, different types of constraints can be included in the formulation of the weighting functions $g_i(\mathbf{c})$. In particular, we could include triple-constraints by modifying the weighting function to be:

$$\begin{aligned}
g_i(\mathbf{c}) &= \prod_{j,k \neq i} \exp(\mathbf{W}_{i,j,k} \delta_{\mathbf{c}_i \mathbf{c}_j \mathbf{c}_k}) \\
&\text{with } \mathbf{W} \in \mathbb{R}^{N \times N \times N} \text{ symmetric.}
\end{aligned} \tag{30}$$

where $\mathbf{W}_{i,j,k} = 0$ if we do not have any prior information, $\mathbf{W}_{i,j,k} > 0$ indicates that the samples \mathbf{x}_i , \mathbf{x}_j and \mathbf{x}_k should be clustered together and $\mathbf{W}_{i,j,k} < 0$ if they should belong to different clusters. The analysis of these different constraints formulation is outside the scope of our work but they may represent interesting directions for future work.

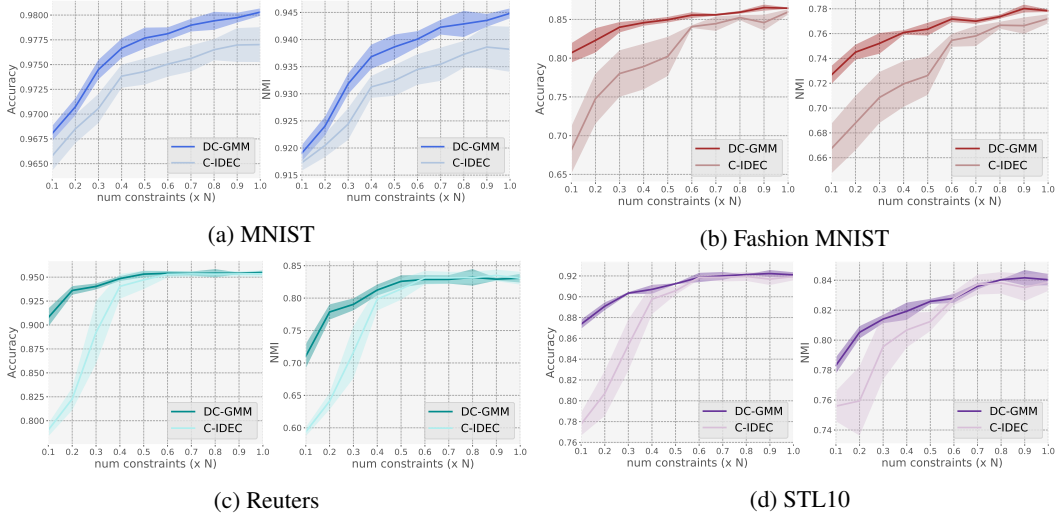


Figure 6: Clustering performance on four different data sets with the number of constraints varying between $0.1 \times N$ and N , where N is the length of the data set. Accuracy and NMI are used as evaluation metrics.

D SCDC Comparison

We perform a through comparison with the SCDC baseline. For a fair comparison we modified the provided code (Luo et al., 2018) to include 6000 constraints to match the setting of the rest of the baselines. In Table 3 we report the accuracy, Normalized Mutual Information (NMI), and Adjusted Rand Index (ARI) for MNIST (LeCun et al., 2010) and Fashion MNIST (Xiao et al., 2017). As the results were highly unstable, we reported only the best performance over 10 runs. The code provided by the authors performed very poorly on the Reuters and the STL-10 data sets as it has been optimized for the MNIST dataset, hence we decided to exclude them.

Table 3: Clustering performances of SCDC (Luo et al., 2018) with 6000 pairwise constraints. The maximum value is computed across 10 runs with different random model initialization.

Dataset	Acc	NMI	ARI
MNIST	70.9	81.0	72.4
FASHION	51.0	59.6	39.5

E Further Experiments

E.1 Different number of constraints

We plot the clustering performance in terms of accuracy and Normalized Mutual Information using a varying number of constraints, N_c , in Figure 6. We observe that our method outperforms C-IDEDEC by a large margin on all four data sets when fewer constraints are used. When N_c gets close to N , the two methods tend to saturate on the Reuters and STL data sets.

E.2 Noisy Labels

In Fig 7, we present the results in term of Accuracy and Normalized Mutual Information of both our model, DC-GMM, and the strongest baseline, C-IDEDEC with N noisy constraints. In particular, the results are computed for $q \in \{0.1, 0.2, 0.3\}$, where q determines the fraction of pairwise constraints with flipped signs (that is, when a must-link is turned into a cannot-link and vice-versa).

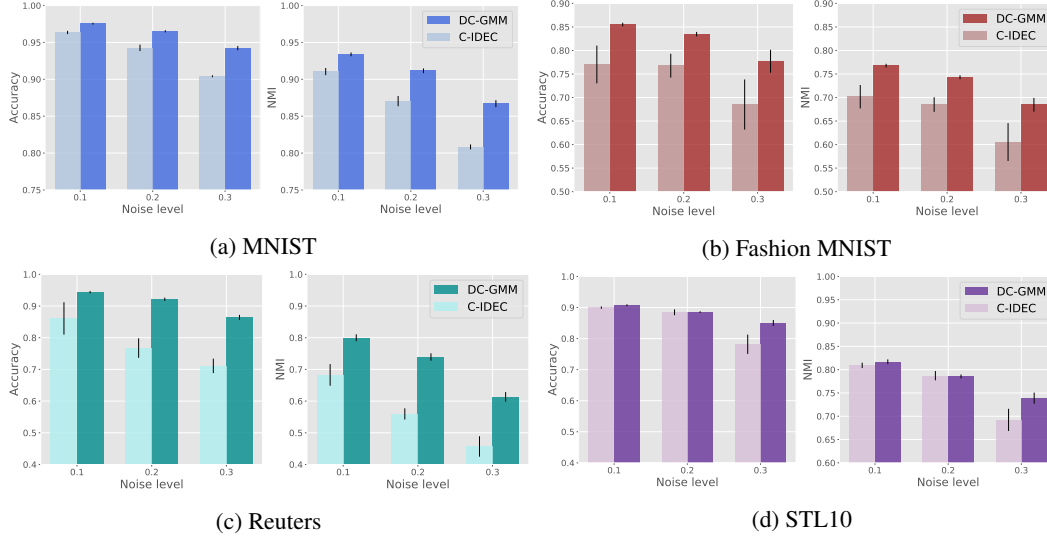


Figure 7: Accuracy and NMI clustering performance on four different data sets with noisy labels.

E.3 Face Image Generation

We evaluate the generative capabilities of our model using the UTKFace data set (Zhang et al., 2017). Using the multivariate Gaussian distributions of each cluster in the learned embedded space, we test the generative capabilities of our method, DC-GMM, by first recovering the mean face of each cluster, and then generating several more faces from each cluster. Figure 8 shows these generated samples. As can be observed, the ethnicities present in the data set are represented well by the mean face. Furthermore, the sampled faces all correspond to the respective cluster, and have a good amount of variation. The quality of generated samples could be improved by using higher resolution training samples or different CNN architectures.



Figure 8: Mean face and sampled faces for each learned cluster, top two rows corresponding to gender, bottom rows to ethnicity

F Implementation Details

F.1 Hyper-parameters setting

In Table 4 we specify the hyper-parameters setting of our model, DC-GMM. Given the semi-supervised setting, we did not focus in fine-tuning the hyper-parameters but rather we chose standard

configurations for all data sets. The learning rate is set to 0.001 and it decreases every 20 epochs with a decay rate of 0.9. Additionally, we observed that our model is robust against changes in the hyper-parameters.

Table 4: Hyperparameters setting of our model, DC-GMM.

	MNIST	FASHION	REUTERS	STL10
Batch size	256	256	256	256
Epochs	1000	500	500	500
Learning rate	0.001	0.001	0.001	0.001
Decay	0.9	0.9	0.9	0.9
Epochs decay	20	20	20	20

F.2 Heart Echo

In addition to the model described in Section 4, we also used a VGG-like convolutional neural network. This model is implemented in Tensorflow, using two VGG blocks (using a 3×3 kernel size) of 32 and 64 filters for the encoder, followed by a single fully-connected layer reducing down to an embedding of dimension 10. The decoder has a symmetric architecture.

The VAE is pretrained for 10 epochs, following which our model is trained for 500 epochs using the same hyper-parameters of Table 4. Refer to the accompanying code for further details.

F.3 Face Image Generation

The face image generation experiments using the UTK Face data set described in Section 4 were carried out using VGG-like convolutional neural networks implemented in Tensorflow. In particular, the input image size of $64 \times 64 \times 3$ allowed two VGG blocks (using a 3×3 kernel size) of 64 and 128 filters for the encoder, followed by a single fully-connected layer reducing down to an embedding of dimension 50. The decoder has a symmetric architecture.

The VAE is pretrained for 10 epochs, following which our model is trained for 1000 epochs using a batch size of 256, a learning rate of 0.001 that decreases every 50 epochs with a decay rate of 0.9. Refer to the accompanying code for further details.

F.4 Resource Usage

Experiments were conducted on an internal computing cluster. Each experiment configuration used one NVIDIA GPU (either a 1080TI or 2080TI), 4 CPUs and a total of 20GB of memory.